Modified higher-order wake oscillator model for vortex-induced vibration of circular cylinders

A. Farshidianfar & N. Dolatabadi

Acta Mechanica

ISSN 0001-5970
Volume 224
Number 7

Acta Mech (2013) 224:1441-1456
DOI 10.1007/s00707-013-0819-0

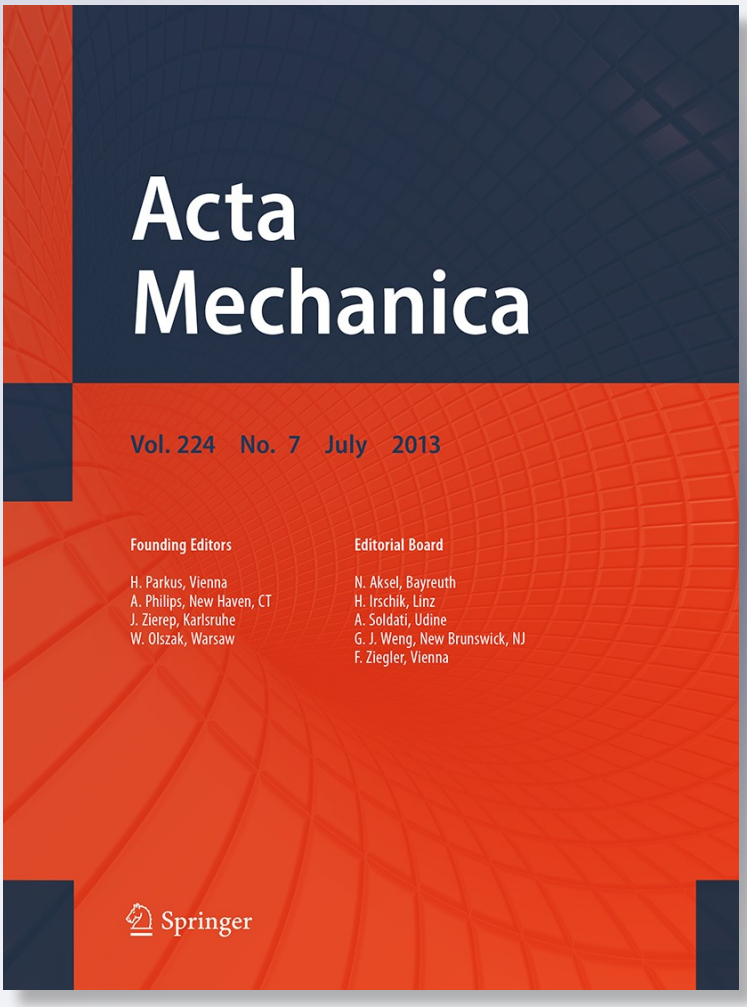

Springer

Acta Mech 224, 1441–1456 (2013)
DOI 10.1007/s00707-013-0819-0

A. Farshidianfar · N. Dolatabadi

Modified higher-order wake oscillator model for vortex-induced vibration of circular cylinders

Received: 12 February 2012 / Revised: 28 August 2012 / Published online: 12 February 2013

Abstract In the present study, a modified model is introduced to estimate the structural oscillation amplitude of a circular cylinder during lock-in in the vortex-induced vibration phenomenon. The modified model includes the same van der Pol term as in the classic model, while its coefficients are assumed to be variable. This modified model is utilized to bring about compliance between theoretical solution and experimental results. Then, a fifth-order aerodynamic term is added, and the coefficients are modified and optimized using a new straightforward solution method. Here, the displacement, velocity and acceleration coupling terms are used to solve the system of equations. The response of the coupled equations is assumed to be harmonic. A linear approach is adopted to simplify and derive the solutions algebraically. The results are plotted during lock-in for amplitude as a function of reduced velocity and for maximum structural oscillation amplitude versus Skop–Griffin parameter. Finally, these results are compared with those of the classic wake oscillator model. The present modified model evinces an exact compliance with experimental measurements regarding structural oscillation amplitude, lock-in range, some hysteresis and mass damping ratio attributes, and reduces sensitivity to the type of coupling term through adding the fifth-order damping term.

List of symbols

A	Force coefficient defined through experiment
b	Constant for damping term in Landl model
C_D	Drag coefficient
C_L	Lift coefficient
C_{L0}	Reference lift coefficient
C_M	Added-mass coefficient
D	Cross-section diameter of cylinder
F	The effect of cylinder on the wake
f	Dimensionless F
h	Support stiffness
K	Lift magnification factor
M	Mass number
m	Structure mass plus fluid added-mass
m_f	Fluid added-mass

A. Farshidianfar · N. Dolatabadi (✉)
Department of Mechanical Engineering,
Ferdowsi University of Mashhad, Mashhad, Iran
E-mail: nadder.dolatabadi@gmail.com; N.Dolatabadi@lboro.ac.uk
Tel.: +44-744-8889844

m_s	Structure mass
q	Reduced vortex lift coefficient
q_0	Reference limit-cycle amplitude of wake oscillator
r	Damping coefficient of the system
r_f	Fluid added-damping
r_s	Dissipation in structure and support
S	The effect of near wake on the structure
S_G	Skop–Griffin number
St	Strouhal number
s	Dimensionless S
T	Time variable
t	Dimensionless time variable
U	The velocity of ambient flow
U_r	Reduced velocity of flow
$u(t)$	Linear part of q
$v(t)$	Nonlinear part of q
Y	Structural oscillation transverse to the flow
y	Dimensionless Y
y_0	Amplitude of y
$y_{M,a}$	Maximum y for acceleration coupling
$y_{M,d}$	Maximum y for displacement coupling
$y_{M,v}$	Maximum y for velocity coupling

Greek letters

α'	Damping coefficient for zero-order term in Landl model
β	β' over nonlinear coefficient ε
β'	damping coefficient for second-order term in Landl model
γ	Stall parameter
δ	Reduced angular frequency of structure
ε	Coefficient of nonlinearity
λ	λ' over nonlinear coefficient ε
λ'	Damping coefficient for fourth-order term in Landl model
μ	Dimensionless mass ratio
ξ	The structural reduced damping coefficient
ρ	Fluid density
Ω	Reference frequency
Ω_f	Vortex shedding angular frequency
Ω_s	Structural angular frequency
Ω_r	Reduced frequency of structure for Landl model
ω_0	The frequency of wake oscillator for harmonic solution to the linear part of q

1 Introduction

Vortex-induced vibration (VIV) is a self-regulated nonlinear phenomenon that shows up in many engineering situations such as offshore structures, aircraft control surfaces, bridges, heat exchangers, chimneys, power transmission lines and other hydrodynamic and hydro-acoustic applications. A cylinder experiences six degrees of freedom motion during VIV which is often reduced to one transverse motion, if it is not fixed. The transverse motion of the cylinder is due to a fluctuating lift force on it which, in turn, is originated from shedding vortices beyond the bluff body. When the shedding frequency of vortices is locked into the natural frequency of the structure, the amplitude of oscillation drastically increases. Therefore, study of VIV turns out to be crucial to either avoid unpredictable destructions or utilize the oscillation to generate power as an aquatic clean energy source.

There are different approaches to the study of VIV which are experimental studies, semi-empirical models and numerical methods [1]. Literature is rife with many experimental works, especially for circular cylinders. One can seek details on this category in the works of Bearman [2], Sarpkaya [3], Khalak and Williamson [4], Williamson and Roshko [5], Zdrakovich [6] and Williamson [7]. More information on numerical methods is

introduced in works of Bearman [8], Sarpkaya [9,10], Evangolinos et al. [11] and Zhou et al. [12]. The main purpose of this paper lies in the category of semi-empirical models; thus, further consideration on this issue is performed.

Semi-empirical models can be classified into three main types for structures undergoing vortex-induced vibration. The first class includes wake oscillator–coupled models which are core subject of this paper. These models represent body and wake oscillator equations coupled through common terms. Investigation of these models is available in the works of Bishop and Hassan [13], Hartlen and Currie [14], Griffin et al. [15] and Skop and Griffin [16]. The second and third classes are single degree of freedom (sdof) and force decomposition models, respectively, which contain a single equation. The former has aeroelastic forcing terms on the right-hand side of the equation, while the latter relies on the measurement of components of forces based on their origins.

Several wake oscillator models have been introduced to describe VIV and lock-in phenomena. The most successful model is van der Pol or so-called classic model regarding structural oscillation behavior [17,18]; however, it is not in exact compliance with experimental results. Farshidianfar and Zanganeh [19] assumed a van der Pol structural damping term which is the same as wake oscillator damping term. Their model follows experimental results to a good deal even though it intensifies the complexity of the problem due to numerical methods used to solve frequency equations. All wake oscillator models are sensitive to the coupling term which is introduced in the form of displacement, velocity or acceleration.

Having known the fact that van der Pol wake oscillator is the best model among wake oscillator models which is introduced in the literature till the present time [1], a modified model is introduced based on classic wake oscillator and Landl models with the assumption of some variable coefficients. This modified model is exploited to obtain a general graph which reveals the values of variable coefficients for which both classical and modified models have limit-cycle behavior. The classical model is then optimized and modified to follow experimental results through setting a proper coefficient using this graph. Finally, the influence of a fifth-order aerodynamic damping term, related to Landl model [20], is observed on the modified classical model with the exception that our purpose is modification of oscillation amplitude rather than consideration of hysteretic effects. The combination of these three steps results in final modified model whose compliance with experimental results is pinpointed and compared with the work of Facchinetti and de Langre [18]. Also, the sensitivity of the recently introduced model to the coupling terms is discussed.

2 VIV model

2.1 Structure oscillator

Let us assume a rigid circular cylinder of diameter, D, which is elastically supported and is free to oscillate transverse to the fluid flow (Fig. 1). The dimensional displacement equation of the structure is considered to be linear as follows:

$$mY'' + rY' + hY = S. \tag{1}$$

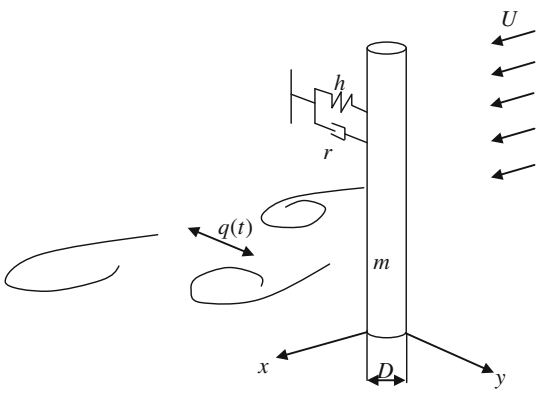

Fig. 1 Model of coupled structure and wake oscillators for 2-D vortex-induced vibrations: U ambient velocity; m structure mass plus fluid added-mass; h support stiffness; r damping of system; D diameter of circular cylinder; $q(t)$ reduced vortex lift coefficient

S on the right-hand side of Eq. (1) indicates the forcing parameter which couples the effect of vortices on the structure. It suffices to introduce S schematically here as it will be explored later in a dimensionless form of s. Primes over Y indicate derivatives with respect to dimensional time T. m consists of both structural mass, m_s, and fluid added-mass m_f. The damping term r includes dissipations in the support r_s and the fluid added-damping r_f [21]. h is the linear stiffness. These parameters are given in detail as follows:

$$\begin{aligned} m &= m_s + m_f, \quad m_f = C_M \rho D^2, \mu = (m_s + m_f)/\rho D^2, \\ r &= r_s + r_f, \quad r_f = \Omega \gamma \rho D^2, \end{aligned} \tag{2}$$

where ρ, μ and C_M are, respectively, fluid density, dimensionless mass ratio and added-mass coefficient. γ is the stall parameter and indicates the added-damping coefficient of cross-flow fluid [22,23]. This parameter depends on the structure velocity and will be mathematically explained later in the present paper. Ω is a reference frequency which is equal to vortex shedding angular frequency, $\Omega_f = 2\pi St U/D$, where St is the Strouhal number. Strouhal number is used to identify the vortex shedding frequency of a body at rest [24]. Defining the structural angular frequency $\Omega_S = (h/m)^{0.5}$ and the structure reduced damping $\xi = r_s/(2m\Omega_s)$, we can rewrite Eq. (1) as:

$$Y'' + \left(2\xi\Omega_s + \frac{\gamma}{\mu}\Omega_f\right) Y' + \Omega_s^2 Y = S/m. \tag{3}$$

2.2 Wake oscillator

The wake oscillator models the nonlinear behavior of vortices which are fluctuating with limited amplitude. The classical and modified models are discussed in this section.

2.2.1 Classical model

The idea of the classical model is inspired from van der Pol equation which is worked out by Nayfeh [17] and reads

$$q'' + \varepsilon\Omega_f (q^2 - 1) q' + \Omega_f^2 q = F, \tag{4}$$

where q is a dimensionless wake variable which is interpreted as the reduced vortex lift coefficient. The following relation reveals the wake variable as a function of the lift coefficient:

$$\frac{q}{q_0} = \frac{C_L}{C_{L0}}. \tag{5}$$

Here, C_{L0} is the reference lift coefficient of a fixed cylinder subjected to vortex shedding, and q_0 is equal to 2 as a result of mixed-secular term elimination through straightforward method [17]. q_0 shows the finite amplitude of a stable quasi-harmonic oscillation, when $F = 0$ and $0 < \varepsilon \ll 1$. F represents the effect of cylinder motion on the wake, while the wake oscillator is expressed as a function of dimensional time T. This parameter will change into f using dimensionless time t. ε is a nondimensional tuning coefficient which reflects the degree of nonlinearity of the system. The quantity of this parameter is obtained through the nonlinear behavior of wake oscillator and is defined here according to the previous work of Facchinetti and de Langre [18], where it is shown that the value of this parameter is almost unchanged and equal to 0.3. C_L is the vortex lift coefficient and varies with time.

Prior to coupling of structure and wake oscillator equations, time T and displacement Y are required to be reduced to dimensionless form. Thus, we introduce some variables such as $t = T\Omega_f$ and $y = Y/D$. Consequently, the dimensionless equations are coupled as:

$$\begin{aligned} &\ddot{y} + \left(2\xi\delta + \frac{\gamma}{\mu}\right)\dot{y} + \delta^2 y = s, \\ &\ddot{q} + \varepsilon(q^2 - 1)\dot{q} + q = f, \end{aligned} \tag{6}$$

where over dots indicate derivatives with respect to dimensionless time. δ is the reduced angular frequency of the structure, Ω_s/Ω_f, and can also be defined as:

$$\delta = \frac{1}{StU_r}, \quad U_r = \frac{2\pi}{\Omega_s}\frac{U}{D}, \tag{7}$$

where U is the ambient velocity of flow and its dimensionless form, known as reduced velocity, is given by U_r.

The effect of the near wake on the structure is given by s as a function of fluctuating lift force C_L [14]. In dimensionless form, it is shown as:

$$s = Mq, \quad M = \frac{C_{L0}}{2}\frac{1}{8\pi^2 St^2\mu}. \tag{8}$$

As μ is introduced to be mass ratio, M indicates the mass number [18]. f as explained before models the coupling between structural displacement y and wake oscillation. The focus of several papers has been on the determination of f in order to achieve the compliance between analytical results of the coupled equations and experimental measurements. Hartlen and Currie [14] were the pioneers to use velocity as the coupling term. Facchinetti and de Langre considered two displacement and acceleration coupling terms besides the velocity term using van der Pol wake oscillator. Thus, the same trend is performed here, and the three coupling terms are investigated simultaneously. A is a parameter which is defined through fitting of transfer function model responses of the wake oscillator to experimental data [18]. The numerical value of A is discussed in the upcoming sections.

$$f = Ay \text{ or } A\dot{y} \text{ or } A\ddot{y}. \tag{9}$$

2.2.2 Modified model

The modified model is inspired from the work of Landl [20]. This model consists of a van der Pol damping term and a fifth-order aerodynamic damping term which is given as:

$$\ddot{C}_L + (\alpha' - \beta' C_L^2 + \lambda' C_L^4)\dot{C}_L + \Omega_r C_L = b\dot{y}. \tag{10}$$

Here, Ω_r is the reduced frequency of the structure and α', β', λ' and b are constants which can be chosen independently to approximate a given problem [20]. Damping terms are sampled and used in the modified model. Since a comparison between van der Pol and modified wake oscillator is desired, it is assumed that $\alpha' = \varepsilon$, $\beta'/\varepsilon = \beta$ and $\lambda'/\varepsilon = \lambda$. Then, Eq. (10) turns to Eq. (11) by extracting the cofactor ε, inserting Eq. (5) into it and considering a general force term f,

$$\ddot{q} + \varepsilon(1 - \beta q^2 + \lambda q^4)\dot{q} + \Omega_r q = f. \tag{11}$$

Up to now, the Landl model is modified, but Ω_r will be neglected to keep the attributes of the newly modified model intact in comparison with the main classical model, Eq. (6). Consideration of Ω_r is not treated in this paper; however, one can expand the current trend studying the effect of reduced frequency ratio. Consequently, as it is desired, the only effectual parameter that can paste any changes in the behavior of the wake oscillator is the fifth-order damping term. Therefore, the final modified equation is introduced as:

$$\ddot{q} + \varepsilon(1 - \beta q^2 + \lambda q^4)\dot{q} + q = f. \tag{12}$$

As a sequel to Facchinetti and de Langre's paper [18], this higher-order model is studied substituting each of displacement, velocity and acceleration coupling terms in Eq. (9) for f.

3 Study of coefficients

A straightforward method is adopted by Nayfeh to solve the van der Pol equation and eliminate the mixed-secular term which is responsible for the divergent behavior of classical wake oscillator [17]. The coefficients are constant in classical van der Pol model; therefore, a single value of q_0 limits the oscillation amplitude to the value of 2. On the other hand, the modified model includes variable coefficients. The same straightforward method is utilized here to specify appropriate values of coefficients such that the mixed-secular term is discarded. This procedure yields a set of curves that can be generalized to both the classical and the modified wake oscillators because if $\lambda = 0$, the modified model reduces to the classical oscillator with a variable coefficient β.

3.1 Straightforward solution

According to Nayfeh [17], we can rewrite the modified wake oscillator as:

$$\ddot{q} + q = \varepsilon(-1 + \beta q^2 - \lambda q^4)\dot{q}. \tag{13}$$

It is assumed that the solution to the wake oscillator is decomposed into linear and nonlinear parts. Higher-order nonlinearities are neglected,

$$q(t, \varepsilon) = u(t) + \varepsilon v(t) + \cdots \tag{14}$$

Substituting Eq. (14) into Eq. (13), we can solve linear and nonlinear parts separately. These parts are shown in Eq. (15):

$$\ddot{u} + u = 0, \quad \ddot{v} + v = -\dot{u} + \frac{\beta}{3}\dot{u}^3 - \frac{\lambda}{5}\dot{u}^5. \tag{15}$$

Exerting some algebraic computations, the solutions to Eq. (15) are obtained as:

$$\begin{aligned} u &= q_0 \cos(\omega_0 t), \\ v &= -\frac{1}{2}\left(1 - \frac{\beta}{4}q_0^2 + \frac{\lambda}{8}q_0^4\right) q_0 t \cos(\omega t) - \frac{1}{8}\left(\frac{\beta}{12} - \frac{\lambda}{16}q_0^2\right) q_0^3 \sin 3(\omega t) - \frac{\lambda}{1920} q_0^5 \sin 5(\omega t). \end{aligned} \tag{16}$$

The final solution to the wake oscillator is the combination of linear and nonlinear parts, u and v. Since the mixed-secular term is responsible for a divergent behavior of the model, it is desirable to eliminate it [17]. The elimination of this term results in a fourth-order equation which defines a set of curves with limit-cycle behavior. The positive answers to the fourth-order equation are represented in Eq. (17),

$$q_{0,1} = \sqrt{\frac{\frac{2\beta}{\lambda} + \left(\left(\frac{2\beta}{\lambda}\right)^2 - \frac{32}{\lambda}\right)^{0.5}}{2}}, \quad q_{0,2} = \sqrt{\frac{\frac{2\beta}{\lambda} - \left(\left(\frac{2\beta}{\lambda}\right)^2 - \frac{32}{\lambda}\right)^{0.5}}{2}}. \tag{17}$$

3.2 Graphical analysis

Having defined a set of curves for which the amplitude of fluctuations is limited, we introduce a graph which depicts q_0 as a function of coefficient λ for different arbitrary β's (Fig. 2). The lines in dashed format show

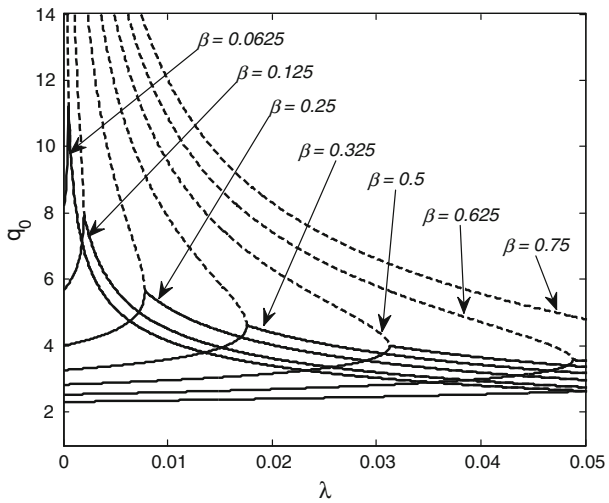

Fig. 2 q_0 as a function of coefficient λ for different values of β's: plots show the values of parameters for limit-cycle wake oscillator

Table 1 Values of coefficients read from bifurcation points of the graphs in Fig. 2

β	λ	q_0
0.0625	0.0005	11.21
0.125	0.002	7.929
0.25	0.008	5.581
0.5	0.032	3.96
0.75	0.071	3.252
1	0.125	2.828
1.25	0.196	2.526
1.5	0.282	2.307
1.75	0.383	2.137
2	0.5	2

$q_{0,1}$'s with positive sign in the square root, and boldfaced lines indicate $q_{0,2}$'s with negative sign. If we set $\lambda = 0$ in Eq. (12), the modified model turns into the classic oscillator. Therefore, this graph is generalized and the effect of variable coefficients can be studied for both models.

On the right-hand side of bifurcation points, both q_0 responses converge and precisely lie on each other while the maximum amplitude of the wake oscillator slopes down. As β decrease, these bifurcation points shift to the left and are located on smaller λ's. On the left-hand side of bifurcation points, there is a discrepancy between $q_{0,1}$'s and $q_{0,2}$'s. It can be concluded that just $q_{0,2}$'s are in compliance with the behavior of the classic wake oscillator as λ leads to zero. The maximum structural oscillation amplitude of the classic model is smaller than the experimental results according to the Skop–Griffin plot [22] represented by Facchinetti and de Langre [18,32]. As the graph reveals, this maximum amplitude can be optimized through reduction in β while $\lambda = 0$. Hence, an appropriate β should be sought through the consideration of van der Pol model. Even more optimization is predicted through inserting λ such that the modified wake oscillator is located on the bifurcation point as a peak. More values of coefficients and the wake oscillator amplitude for the bifurcation peaks are given in Table 1.

4 Values of parameters

The parameters for the classical wake oscillator are defined through experimental data on vortex shedding behind cylinders. These parameters are benefitted for the modified model as well, because the same parameters are required to establish a comparison between the recently introduced model and the previous one.

The reduced damping ξ and mass number M, as given quantities, are equal to 3.1×10^{-3} and 2×10^{-4}, respectively [25]. δ is also a given parameter that depends on the Strouhal number St and the reduced velocity U_r [18]. The parameter C_{L0} is usually taken as $C_{L0} = 0.3$ in the large range of Re [21,26]. The Strouhal number can be assumed as $St = 0.2$ for the subcritical range of $300 < Re < 1.5 \times 10^5$ [21,26]. Substitution of these values into the mass number, Eq. (8), yields a relation for mass ratio μ,

$$\mu = \frac{0.05}{M}. \tag{18}$$

The fluid added-damping coefficient γ, which is introduced in Eq. (2), is a function of the drag coefficient of the structure and is given as

$$\gamma = \frac{C_D}{4\pi St}. \tag{19}$$

For the subcritical range of Re, C_D depends on the structure transverse motion and is defined as $(1+2y_0)C_{D0}$ [21,26]. For simplicity, we assume here a constant amplified drag coefficient $C_D = 2.0$, so that from Eq. (19) $\gamma = 0.8$ [18].

Vickery and Watkins [27], Bishop and Hassan [13], King [28], Griffin [29] and Pantazopolous [26] set out experiments to plot lift magnification, K, versus structural amplitude, y_0. This plot is studied by Facchinetti and de Langre [18] to find the best proportion of A/ε for all acceleration, velocity and displacement conditions. A and ε are introduced in Sect. 2.2.1. They concluded that $A/\varepsilon = 40$ best fits the experimental data, where A should be equal to 12 because ε is almost unchanged and equal to 0.3.

5 Dynamical study of VIV

In this section, we investigate the derivation of dominant dynamical equations of wake oscillator. These equations are given for the classic model by Facchinetti and de Langre [18]; therefore, we just exploit them to establish a classic wake oscillator equation with variable coefficient and modified through β. Details on the dynamics of displacement and velocity couplings are described in Krenk and Nielsen [30] and Balasubramanian and Skop [22], respectively. In both models introduced here, a solution is sought in the form of

$$y(t) = y_0 \cos(\omega t), \quad q(t) = q_0 \cos(\omega t - \phi), \tag{20}$$

where the structure and the fluid signals admit time-independent common angular frequency ω, amplitudes q_0, y_0, and relative phase ϕ [18].

5.1 Classic model modified through β

First, we consider the classic wake oscillator model with a variable coefficient β. Thus, the dynamical equations, which are derived by Facchinetti and de Langre [18], will remain untouched except for amplitude q_0 where β is playing a key role. These four equations of amplitude and phase of the linear transfer function between the structure displacement and fluid variable, amplitude q_0 and the angular frequency ω are given as follows:

$$\frac{y_0}{q_0} = \frac{M}{\sqrt{(\delta^2 - \omega^2)^2 + (2\xi\delta + \frac{\gamma}{\mu})^2 \omega^2}}, \tag{21}$$

$$\tan\phi = \frac{-(2\xi\delta + \gamma/\mu)\omega}{\delta^2 - \omega^2}, \tag{22}$$

$$q_0 = \frac{2}{\sqrt{\beta}} \sqrt{1 + \frac{AM}{\epsilon} \frac{C}{\left(\delta^2 - \omega^2\right)^2 + \left(2\xi\delta + \frac{\gamma}{\mu}\right)^2 \omega^2}}, \tag{23}$$

$$\omega^6 + \left[1 + 2\delta^2 - \left(2\xi\delta + \frac{\gamma}{\mu}\right)^2\right]\omega^4 - \left[-2\delta^2 + \left(2\xi\delta + \frac{\gamma}{\mu}\right)^2 - \delta^4\right]\omega^2 - \delta^4 + G = 0, \tag{24}$$

where the factors C and G are defined based on the coupling term. For displacement, velocity and acceleration couplings, these parameters, respectively, read as follows:

$$C = -(2\xi\delta + \gamma/\mu), \quad G = AM\left(\delta^2 - \omega^2\right), \tag{25}$$

$$C = \delta^2 - \omega^2, \quad G = AM\,(2\xi\delta + \gamma/\mu)\,\omega^2, \tag{26}$$

$$C = (2\xi\delta + \gamma/\mu)\,\omega^2, \quad G = AM\left(\omega^2 - \delta^2\right)\omega^2. \tag{27}$$

Figure 3 depicts the frequency response of fluid structure equations for these three displacement, velocity and acceleration couplings. As it is clearly seen, lock-in occurs at $U_r = 1/St$ where $\omega = \delta = 1/(StU_r)$. Displacement and acceleration frequency responses are almost symmetric. For velocity coupling, this trend is asymmetric, and lock-in starts at reduced velocities higher than $U_r = 1/St$, while at lower reduced velocities, there exist only lock-out states. All three couplings are locked onto the structure common frequency $\omega = 1$. The investigation of present data reveals that displacement and acceleration couplings span the lock-in domain truly and follow its intrinsic behavior more accurately than velocity coupling.

Let us consider the wake oscillator amplitude now. The classic oscillator sets itself on the limit cycle of amplitude $q_0 = 2$; however, based on the optimized model through coefficient β, this value has changed. As it is shown, there are various values of β one can choose to set a limit-cycle coupled system. These values are substituted in responses, and it is spotted that the best value that brings about compatibility between mathematical model and experimental measurements is $\beta = 0.0625$. Since this parameter is specified mathematically, its relation to the physical parameters of the coupled system remains in question and can be sought as a separate research. The selected value of β can be used in almost any problem experimented in water or air, because the experimental data which are used to determine β pertain to these fluids and are amassed from different experiments under diverse conditions. Having selected $\beta = 0.0625$, the wake oscillator amplitude is set on

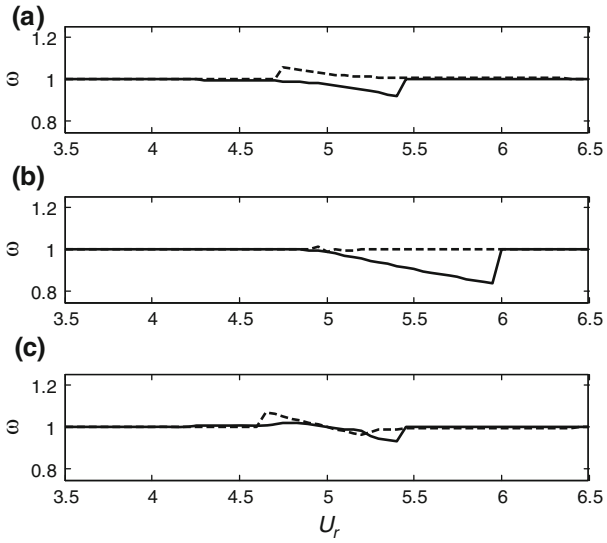

Fig. 3 Angular frequency ω as a function of reduced velocity U_r: **a** displacement coupling; **b** velocity coupling; **c** acceleration coupling. Increasing U_r, *solid line*; decreasing U_r, *dashed line*

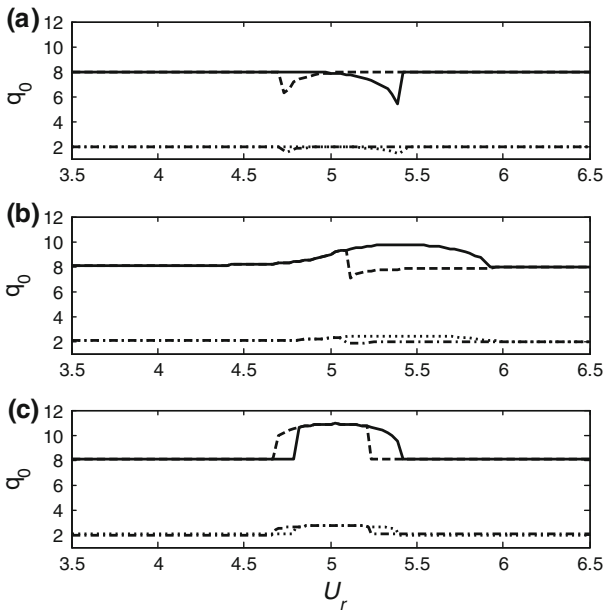

Fig. 4 Amplitude of wake oscillator q_0 as a function of reduced velocity U_r: **a** displacement coupling; **b** velocity coupling; **c** acceleration coupling. Classic oscillator: increasing U_r, *dotted line*; decreasing U_r, *dashed dotted line*. Modified Oscillator through the coefficient β: increasing U_r, *solid line*; decreasing U_r, *dashed line*

$q_0 = 8$ as it is shown in boldfaced lines in Fig. 4. Since this value of q_0 is derived from elimination of the mixed-secular term, as a purpose to set a limit- cycle fluctuation, it varies with β. The modified model through the coefficient β has the same lock-in attributes of classic wake oscillator except that the amplitudes during lock-in are magnified due to this optimization, and they are plotted with classic wake oscillator amplitudes in Fig. 4.

Considering structural oscillation amplitude, Fig. 5, one can easily understand that the modified model enables us to model y_0 more accurately than classic model with respect to experimental results worked out by Parkinson et al. [31] and Khalak and Williamson [4]. These modified results are given in boldfaced lines, while results from the classic wake oscillator are shown by regular (normal) lines (Fig. 5). Velocity and acceleration couplings predict the amplitude of oscillation better than displacement; however, displacement and acceler-

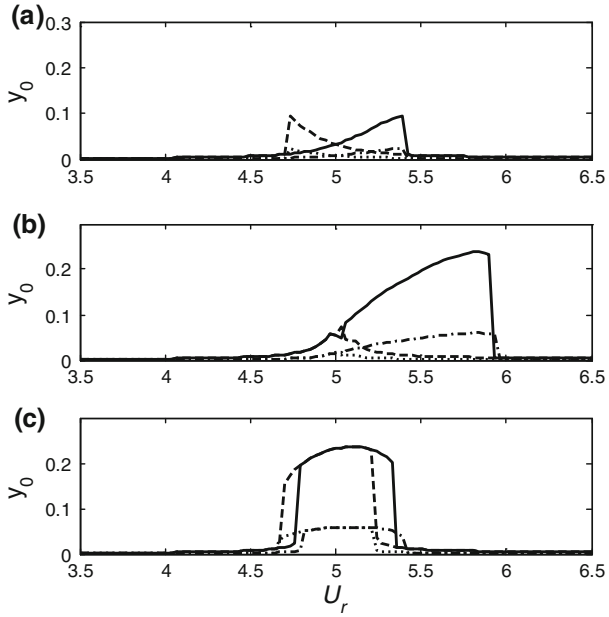

Fig. 5 Amplitude of the structure oscillator y_0 as a function of reduced velocity U_r: **a** displacement coupling; **b** velocity coupling; **c** acceleration coupling. Classic oscillator: increasing U_r, *dashed dotted line*; decreasing U_r, *dotted line*. Modified Oscillator through coefficient β: increasing U_r, *solid line*; decreasing U_r, *dashed line*

ation can model lock-in attributes precisely. Acceleration coupling enables us to present a better compliance with hysteretic effects. Thus, one can analyze that acceleration coupling is the most accurate coupling term compared with displacement and velocity ones.

If we set $\omega = \delta = 1$ in Eqs. (21, 23) and substitute the Skop–Griffin parameter simultaneously, the maximum structural amplitude y_M is obtained for three couplings. The Skop–Griffin parameter S_G is defined as:

$$S_G = 8\pi^2 St^2 \mu\xi = \frac{C_{L0}}{2}\frac{\xi}{M}. \tag{28}$$

Therefore, three displacement, velocity and acceleration maximum structural amplitudes are, respectively, given as:

$$y_{M,\text{disp.}} = \frac{C_{L0}/2}{S_G + 4\pi^2 St^2\gamma}\sqrt{\frac{1}{\beta}\left(1 - \frac{A}{\epsilon}\frac{C_{L0}/4}{S_G + 4\pi^2 St^2\gamma}\right)}, \tag{29}$$

$$y_{M,\text{veloc.}} = \frac{2}{\sqrt{\beta}}, \tag{30}$$

$$y_{M,\text{accel.}} = \frac{C_{L0}/2}{S_G + 4\pi^2 St^2\gamma}\sqrt{\frac{1}{\beta}\left(1 + \frac{A}{\epsilon}\frac{C_{L0}/4}{S_G + 4\pi^2 St^2\gamma}\right)}. \tag{31}$$

In Fig. 6, these equations are plotted in Skop–Griffin graph as a function of Skop–Griffin parameter S_G [15]. The boldfaced graphs show the modified model, and normal lines belong to the classical model. It is clearly distinguished that the modified model is in exact compliance with the experimental results especially for the acceleration model which entirely lies on the experimental data for $S_G < 1$. Velocity coupling touches the margin of Griffin plots in contrary to the displacement model which is unable to describe the trend of the experimental data on these plots. Having compared the recently introduced model with Farshidianfar and Zanganeh's model [19], one can easily understand that both models are able to follow experimental results to a good deal for $S_G < 1$; however, the modified model is easy to handle due to less and simpler computations.

Further discussion on the selection of acceleration coupling can be found in figure 10 of Facchinetti and de Langre's paper [18]. They showed in this figure that the acceleration coupling term can fully match experimental measurements regarding the lock-in range, while the mass parameter varies with reduced velocity. Using

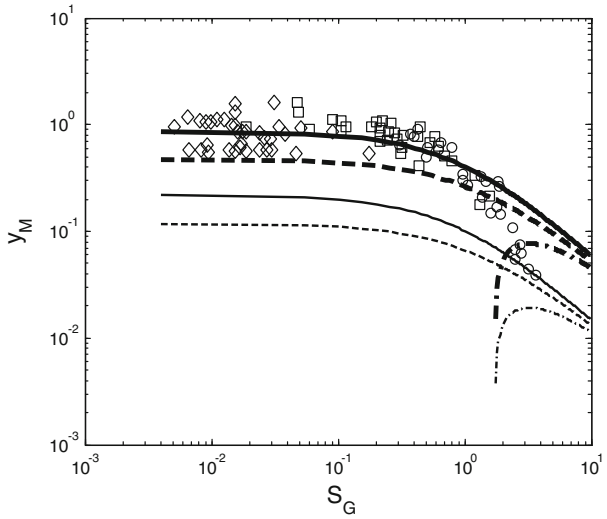

Fig. 6 Maximum structural oscillation amplitude at lock-in y_M as a function of the Skop–Griffin parameter S_G for three displacements, *dashed dotted line*, velocity, *dashed line*, and acceleration, *solid line*, couplings: *boldfaced lines* show modified model, and *regular thin lines* belong to classic van der Pol model. Experimental data in air: *circle* Balasubramanian and Skop [22]. Experimental data in water: *square* Balasubramanian and Skop [22]; *diamond* Khalak and Williamson [4]

the results of our model in contribution with the results of Facchinetti and de Langre, the acceleration coupling term can be selected as the best model to represent vortex-induced vibration attributes. Such contribution is rational, since the only parameter that has been modified so far is the coefficient in van der Pol equation; otherwise, both models are equal.

5.2 Modified model with fifth-order aerodynamic damping term

So far, the classical model has been modified such that the results are in exact compliance with experimental data for a wide range of the Skop–Griffin parameter S_G. According to coefficient graphs in Fig. 2, insertion of the fifth-order aerodynamic damping term modifies the model further. Initially, the dominant equations of higher-order wake oscillator must be derived. Since the structural oscillator equation is untouched, the frequency response will remain the same. Using the same approach of Facchinetti and de Langre [18,32] and using simple algebraic transformations to solve Eq. (12), the wake oscillator amplitude can be given as:

$$q_0 = 2\sqrt{\frac{\beta \pm \sqrt{\beta^2 - 8\lambda\left(1 + \frac{AM}{\epsilon}\frac{C}{(\delta^2-\omega^2)^2+\left(2\xi\delta+\frac{\gamma}{\mu}\right)^2\omega^2}\right)}}{4\lambda}}, \tag{32}$$

where parameter C is the same as in Eqs. (25), (26) and (27) for displacement, velocity and acceleration couplings. Equation (32) introduces two q_0 equations where the difference is the sign of the second square root. q_0 with negative sign truly models the wake oscillator for all λ's, while the positive sign equation is trustworthy for λ's at the right-hand side of the bifurcation point (Fig. 2). q_0 with negative square root sign introduces subtle optimization which is not noticeably effectual. If we pick equivalent λ for bifurcation point and employ q_0 with positive square root sign, more significant modification for the structural oscillation amplitude is obtained. The proper value of coefficient β is found to be 0.0625 from Sect. 5.1. Coefficient λ, which maximizes q_0 for given parameter β, is read from Fig. 2 and $\lambda = 0.0005$. This bifurcation point is of our interest because it reflects the maximum effect of parameter λ on the higher-order damping term where in turn the most significant effect of this higher-order damping term on the whole wake oscillator model is of our interest in this study. The boldfaced graphs belong to the higher-order wake oscillator model in Fig. 7, while regular (normal) graphs pertain to the modified model. The most significant optimization goes to displacement coupling as it is shown; however, the acceleration coupling remains the most successful approach to the modeling of VIV.

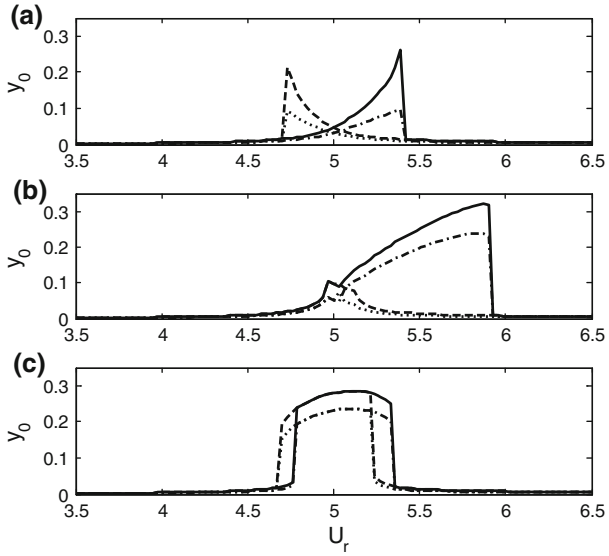

Fig. 7 Amplitude of the structure oscillator y_0 with higher- order wake oscillator damping term as a function of reduced velocity U_r: **a** displacement coupling; **b** velocity coupling; **c** acceleration coupling. Modified oscillator through coefficient β: increasing U_r, *dashed dotted line*; decreasing U_r, *dotted line*. Modified oscillator through higher-order damping term: increasing U_r, *solid line*; decreasing U_r, *dashed line*

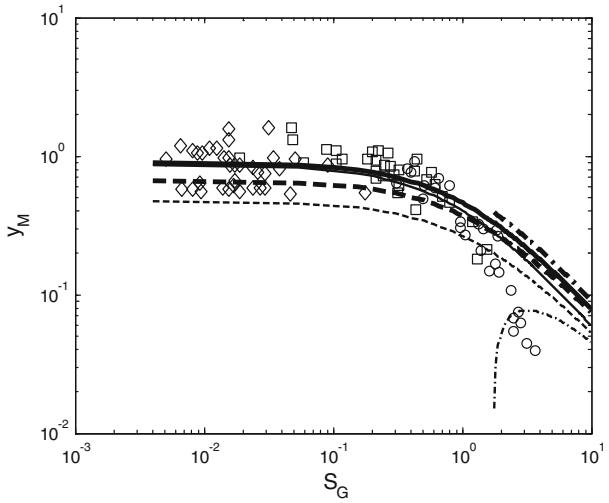

Fig. 8 Maximum structural oscillation amplitude at lock-in y_M as a function of the Skop–Griffin parameter S_G for three displacements, *dashed dotted line*, velocity, *dashed line*, and acceleration, *solid line*, couplings: *Thick lines* show the t_1 modified model with higher-order damping term, and thin lines belong to the modified model through coefficient β. Experimental data in air: *circle* Balasubramanian and Skop [22]. Experimental data in water: *square* Balasubramanian and Skop [22]; *diamond* Khalak and Williamson [4]

Relevant Skop–Griffin plots are given in Fig. 8 through setting $\omega = \delta = 1$. The maximum amplitude equations for three different displacement, velocity and acceleration couplings are derived, respectively, as follows:

$$y_{M,d.} = \frac{C_{L0}/2}{S_G + 4\pi^2 St^2 \gamma} \sqrt{\frac{\beta \pm \sqrt{\beta^2 - 8\lambda \left(1 - \frac{A}{\varepsilon} \frac{C_{L0}/4}{S_G + 4\pi^2 St^2 \gamma}\right)}}{4\lambda}}, \tag{33}$$

$$y_{M,v.} = \frac{C_{L0}/2}{S_G + 4\pi^2 St^2 \gamma} \sqrt{\frac{\beta \pm \sqrt{\beta^2 - 8\lambda}}{4\lambda}}, \tag{34}$$

$$y_{M.a.} = \frac{C_{L0}/2}{S_G + 4\pi^2 St^2 \gamma} \sqrt{\frac{\beta \pm \sqrt{\beta^2 - 8\lambda \left(1 + \frac{A}{\varepsilon} \frac{C_{L0}/4}{S_G + 4\pi^2 St^2 \gamma}\right)}}{4\lambda}}. \tag{35}$$

The maximum oscillation amplitude for the displacement model approximates the acceleration graph for S_G's larger than 1; however, it still fails to follow the experimental data according to Fig. 8. The velocity coupling precisely follows the experimental data since it is in proximity of the acceleration plot (Fig. 8); therefore, we can claim that sensitivity to the coupling term is reduced through application of the higher-order damping term, and deviation between each of displacement, velocity and acceleration plots is minimized; however, the present modified model still fails to predict the experimental data for S_G's larger than one. This is the shortcoming of the current work on which one might be interested to work in future.

6 The effect of mass damping ratio

Up to now, we found that the van der Pol wake oscillator is the best model described in the literature [1]. As a result, we tried to verify our model by comparison with the classic van der Pol model and refused the repetition of these comparisons with previously studied models. We also proved that the acceleration force term can best describe different attributes of the wake oscillator among all three coupling terms. The acceleration coupling term is closer to the real behavior of the wake oscillator with regard to the lock-in range, maximum amplitude and general trend in hysteretic effects; however, it sounds that there are still some discrepancies in the area of hysteresis. In this section, we have a closer look over amplitude and hysteretic behavior of the newly modified model using the acceleration coupling term. Consequently, the analytical result of the amplitude of oscillations is investigated as a function of reduced velocity in comparison with experimental data. These data are represented by Feng [33] for measurements in air and Khalak and Williamson [4] for measurements in water. In other words, the former measurements belong to high mass damping ratio, and the latter belongs to low mass damping ratio systems.

Figure 9 depicts the experimental data for a high mass damping ratio system. The data are provided by Feng [33] for a cylinder in interaction with air medium. We have set the mass damping ratio $m^*\xi$ equal to that of Feng's experiment (0.255) and regenerated the structural oscillation amplitude plot as a function of reduced velocity. The bold regular line pertains to the increase in reduced velocity, and the dashed line is related to the reduction in reduced velocity. Our modified model predicts the amplitude of oscillation to a good extent both quantitatively and qualitatively; however, two deviations are spotted on the graph. Initially, according to the experimental measurement, lock-in occurs at a reduced velocity of 6.0, while in the modified model, it occurs

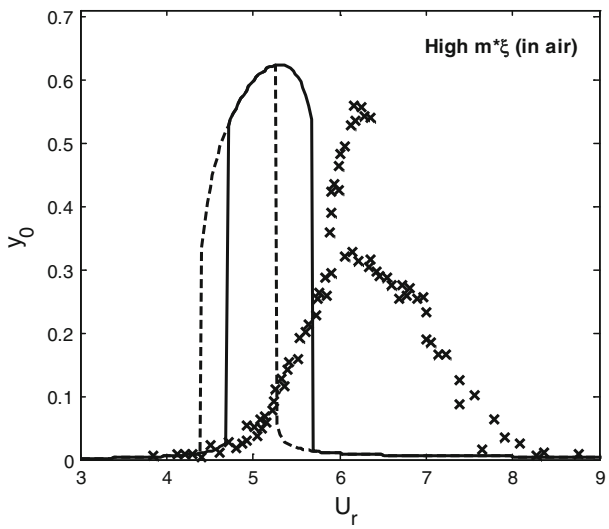

Fig. 9 Oscillation amplitude y_0 versus reduced velocity U_r during lock-in for high mass damping ratio systems. The modified wake oscillator model with acceleration coupling term is compared with experimental data by Feng [33]: increasing U_r, *solid line*; decreasing U_r, *dashed line*; experimental data, *times symbol*

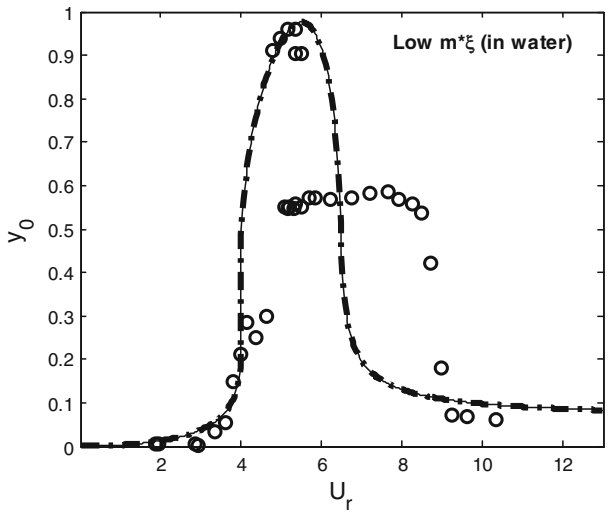

Fig. 10 Oscillation amplitude y_0 versus reduced velocity U_r during lock-in for low mass damping ratio systems. Modified wake oscillator model with acceleration coupling term is compared with experimental data by Khalak and Williamson [4]: increasing U_r, *solid line*; decreasing U_r, *dashed line*; experimental data, *circle*

at the value of 5.0. This discrepancy is not because of the modified model but it is due to the assumption of a constant value for the Strouhal parameter which is set equal to 0.2 in Eq. (7). This selection limits the reduced velocity to 5.0 at which lock-in occurs. In fact, the Strouhal parameter varies with the Reynolds number which in turn is a function of velocity itself. Other simplifications including the assumption of constant stall parameter can be responsible for such error as well, because this parameter is a function of the drag coefficient which apparently varies with time. Consequently, the damping coefficient which is affected by the stall parameter experiences variation from its real value, and it increases the named error. A second deviation occurs during initial excitation and final lock-out. Initiation of lock-in and finalization of lock-out occurs rather smoothly in experimental graph; in the modified wake oscillator model, these shifts occur rather abruptly. In this aspect, the model is incapable of modeling smooth transition. Despite these two shortcomings, one of which is not related to the attributes of the modified model, the modified wake oscillator enables us to capture the exact curvature of transition to maximum structural oscillation amplitude which verifies the power of this wake oscillator model in the study of structural oscillation amplitude during lock-in. Ignoring the abrupt transition during lock-out, the hysteretic effects are acceptable to a good extent compared to the hysteresis plots provided by Gabbai [1].

Figure 10 describes the structural amplitude of oscillation versus reduced velocity for low mass damping ratio systems or systems with mediums like water. To compare the modified model to experimental results, the same mass damping ratio $m^*\xi = 0.013$ is chosen from the experiments of Khalak and Williamson [4]. As it is shown, the model does not experience such deviation which is shown in Fig. 9 during lock-in. The analytical results and experimental points are matching precisely prior to lock-out. Despite smoother lock-out transition for low mass damping ratio, this transition of amplitude still includes the same defection, and lock-out deviation is observed. Hysteretic effects cannot be modeled for low mass damping ratios because both increasing and decreasing graphs of reduced velocity lie on each other. However, other successful features of the model retain its worth in the study of vortex-induced vibrations. It sounds that as the mass damping ratio decreases, the assumption of constant Strouhal and Stall parameters is more realistic and lock-in occurs at the same reduced velocity of 5.0 where the analytic results settle. As it is apparent, the modified model traces the upper branch accurately. As a result, our modified model is suitable to precisely study the behavior of structural oscillation amplitude and specifically upper branch occurrence during lock-in for low mass damping systems.

7 Conclusions

The introduction of a precise low-order model helps to describe the VIV phenomenon with a better physical insight. Different models are studied in the literature since now, but van der Pol is the most successful approach to this goal. Since this model lacks compatibility of results with experimental data with regard to the oscillation amplitude, a new study was performed in the present paper to discard this defect. A modified wake oscillator

model was introduced based on the classical van der Pol model where a coefficient β was utilized to optimize the wake oscillator equation. An appropriate value of $\beta = 0.0625$ was determined for which the maximum structural oscillation amplitude lies on the experimental results. According to the classical model, acceleration coupling still is the best model in all aspects of amplitude, hysteretic effect, and lock-in behavior and range compared to displacement and velocity terms. The influence of the fifth-order aerodynamic damping term on the sensitivity of the model to the coupling term was considered. Based on Skop–Griffin Plots, the coefficient λ is determined based on bifurcation points. Thus, it is simply understood that the higher-order damping term in the wake oscillator model reduces sensitivity to the type of coupling term which can be displacement, velocity or acceleration. The compatibility between analytical results and experimental measurements, as shown in plots, proves that the present model is applicable to both problems with water or air ambient flow about structures.

In general, the presented model enables us to precisely model different attributes of wake and structural oscillations such as lock-in range, maximum amplitude of oscillations, upper branch, excitation of structural oscillation prior to lock-out and with respect to reduced velocity for both high and low mass damping ratios. However, the model is not exact during lock-out. The model is suitable for general studying hysteretic effects for high mass damping ratios. Consequently, the modified wake oscillator model is suitable to study vortex-induced vibrations of structures in both air and water, specifically with oscillation amplitude approaches and to some extent for hysteresis investigations.

As a future work, one can focus on the modification of model parameters such that it will be simultaneously useful for all values of the Skop–Griffin parameter. Moreover, the variable coefficients are mathematically explored to comply with measurements; therefore, one can commence a research to dig into the relation between these values and physical parameters of the coupled system. In spite of the fact that this model is aimed to model oscillation amplitude and its performance and viability is proven, a further study can be commenced to improve the hysteretic effects such that more accurate compliance is achieved for both high and low mass damping ratios.

References

1. Gabbai, R.D., Benaroya, H.: Review: an overview of modeling and experiments of vortex-induced vibration of circular cylinders. J. Sound Vib. **282**, 575–616 (2005)
2. Bearman, P.W.: Vortex shedding from oscillating bluff bodies. Ann. Rev. Fluid Mech. **16**, 195–222 (1984)
3. Sarpkaya, T.: Fluid forces on oscillating cylinders. J. Waterway Port Coast. Ocean Eng. **104**, 275–291 (1978)
4. Khalak, A., Williamson, C.H.K.: Motions, forces and mode transitions in vortex-induced vibrations at low mass damping. J. Fluids Struct. **13**, 813–851 (1999)
5. Williamson, C.H.K., Roshko, A.: Vortex formation in the wake of an oscillating cylinder. J. Fluids Struct. **2**, 355–381 (1988)
6. Zdravkovich, M.M.: Different modes of vortex shedding: an overview. J. Fluids Struct. **10**, 427–437 (1996)
7. Williamson, C.H.K.: the existence of two stages in the transition to three-dimensionality of a cylinder wake. Phys. Fluids **31**, 3165–3168 (1988)
8. Meneghini, J.R., Bearman, P.W.: Numerical simulation of high amplitude oscillatory flow about a circular cylinder. J. Fluids Struct. **9**, 435–455 (1995)
9. Sarpkaya, T.: Computational methods with vortices. J. Fluids Eng. **111**, 5–52 (1989)
10. Sarpkaya, T.: Vortex element methods for flow simulation. Adv. Appl. Mech. **31**, 113–247 (1994)
11. Evangelinos, C.: Parallel Simulation of Vortex-Induced Vibrations in Turbulent Flow: Linear and Non-Linear Models. Brown University, Providence, RI (1999)
12. Zhou, C.Y., So, R.M., Lam, K.: Vortex-induced vibrations of an elastic circular cylinder. J. Fluids Struct. **13**, 165–189 (1999)
13. Bishop, R.E.D., Hassan, A.Y.: The lift and drag forces on a circular cylinder in a flowing fluid. In: Proceedings of the Royal Society (1963)
14. Hartlen, R.T., Currie, I.G.: Lift-oscillator model of vortex-induced vibration. J. Eng. Mech. Div. EM5, 577–591 (1970)
15. Griffin, O.M., Skop, R.A., Koopman, G.H.: The vortex-excited resonant vibrations of circular cylinders. J. Sound Vib. **31**, 235–249 (1973)
16. Skop, R.A., Griffin, O.M.: A model for the vortex-excited resonant response of bluff cylinders. J. Sound Vib. **27**, 395–412 (1973)
17. Nayfeh, A.H.: Introduction to Perturbation Techniques. pp. 147–150. Wiley, New York (1993)
18. Facchinetti, M.L., de Langre, E., Biolley, F.: Coupling of structure and wake oscillators in vortex-induced vibrations. J. Fluids Struct. **19**, 123–140 (2004)
19. Farshidianfar, A., Zanganeh, H.: A modified wake oscillator model for vortex-induced vibration of circular cylinders for a wide range of mass-damping ratio. J. Fluids Struct. **26**, 430–441 (2010)
20. Landl, R.: A mathematical model for vortex-excited vibrations of bluff bodies. J. Sound Vib. **42**, 219–234 (1975)
21. Blevins, R.D.: Flow-Induced Vibrations, vol. 2. Van Nostrand Reinhold, New York (1990)
22. Balasubramanian, S., Skop, R.A.: A new twist on an old model for vortex-induced vibrations. J. Fluids Struct. **11**, 395–412 (1997)

23. Skop, R.A., Luo, G.: An inverse-direct method for predicting the vortex-induced vibrations of cylinders in uniform and nonuniform flows. J. Fluids Struct. **15**, 867–884 (2001)
24. Sarpkaya, T.: A critical review of the intrinsic nature of vortex-induced vibrations. J. Fluids Struct. **19**, 389–447 (2004)
25. Balasubramanian, S., et al.: Vortex-excited vibrations of uniform pivoted cylinders in uniform and shear flow. J. Fluids Struct. **14**, 65–85 (2000)
26. Pantazopoulos, M.S.: Vortex-induced vibration parameters: critical review. In: Proceedings of the 17th International Conference on Offshore Mechanics and Arctic Engineering. Osaka, Japan (1994)
27. Vickery, B.J., Watkins, R.D.: Flow-induced vibration of cylindrical structures. In: Proceedings of the First Australian Conference. Australia University of Western Australia (1962)
28. King, R.: Vortex-excited oscillations of yawed circular cylinders. J. Fluids Eng. **99**, 495–502 (1977)
29. Griffin, O.M.: Vortex-excited cross flow vibrations of a single cylindrical tube. ASME J. Press. Vessel Technol. **102**, 158–166 (1980)
30. Krenk, S., Nielsen, S.R.K.: Energy balanced double oscillator model for vortex-induced vibrations. ASCE J. Eng. Mech. **125**, 263–271 (1999)
31. Parkinson, G.V., Feng, C.C., Ferguson, N.: Mechanism of vortex-induced oscillation of bluff cylinders. In: Symposium on Wind Effects on Buildings and Structures, Loughborough, England, April 1968
32. Farshidianfar, A., Dolatabadi, N., Naranjani, Y.: Consideration of lock-in using a modified wake oscillator in vortex induced vibration about a cylinder. 1st International Conference on Acoustics and Vibration (ISAV 2011), paper 1272, Tehran, Iran, December 2011
33. Feng, C.C.: The measurement of vortex induced effects in flow past stationary and oscillating circular and D-section cylinders. Department of Mechancial Engineering, The University of British Columbia, Canada (1968)